SPE-169126-MS

Synergistic Stabilization of Foams by a Mixture of Nanoparticles and Surfactants

Robin Singh, Kishore K. Mohanty, The University of Texas at Austin

This paper was prepared for presentation at the SPE Improved Oil Recovery Symposium held in Tulsa, Oklahoma, USA, 12–16 April 2014.

Abstract

The goal of this work is to evaluate stabilization of foams by a combination of nanoparticles and surfactants. Hydrophilic silica nanoparticles (NP) and anionic surfactants were used in this study. Static foams were generated using surfactants and surfactant-NP mixtures with and without the presence of a crude oil. The decay of the foam height with time was studied and half-lives were determined. The foam drainage behavior and thickness of the foam lamella were studied by fluorescence microscopy. Aqueous foams were created in-situ by co-injecting the surfactant or surfactant-NP mixtures with nitrogen gas through a Berea sandstone core at a fixed quality. Pressure drop across the core was measured to estimate the achieved mobility reduction factor (MRF). Oil displacement experiments were conducted in Berea cores using surfactant and surfactant-nanoparticle mixture as foaming agents. Static foam tests indicate stabilization effect of nanoparticles on surfactant-nanoparticle foam stability in the absence of crude oil. Lighter crude oils were more destabilizing to foams than heavier oils. Adding nanoparticles even in low concentrations (0.3 wt %) can significantly improve the foam stability and mobility reduction factor in the absence of oil. As the concentration of nanoparticles increased, mobility reduction factor (MRF) of surfactant-nanoparticle foam in a Berea core increased significantly. Fluorescence microscopy elucidated that nanoparticles are trapped in the plateau border as well as lamellas which retard liquid drainage and bubble coalescence. The core floods with a crude oil revealed that the incremental oil recovery by surfactant-NP blend over water flood was about 10% OOIP with an immiscible foam.

Introduction

Gas flooding is the most widely used enhanced oil recovery (EOR) technique (Taber et al., 1997). It comprises injection of enriched-gases and carbon dioxide in waterflooded reservoirs. In US, CO_2-EOR projects alone provide 28,000 barrels of oil per day, which is 5% of the country's oil production (Enick et al., 2012). If the gas is first or multicontact miscible with the oil, it can displace virtually all the oil in the volume swept by the gas (Orr et al., 1982). However, the adverse mobility ratio due to the inherent low viscosity of gas leads to viscous fingering leaving a part of the reservoir uncontacted (Lake et al. 1990). Reservoir heterogeneity, and gravity override also contribute to poor sweep efficiency (Koval, 1963).

Foam can be used to mitigate these problems associated with gas injection (Kovscek et al., 1994; Rossen et al., 2010). The main mechanism by which foam reduces the mobility of gas is by immobilizing or trapping a large fraction of the gas in the porous media, and by increasing the apparent viscosity of gas (Hirasaki and Lawson, 1985). The concept of using foams as mobility control agents was first proposed by Bond and Holbrook (1958). Since then, there have been several successful foam pilot tests in which surfactant and gases were co-injected in reservoir for mobility control (Patzek, 1996). In bulk, foam is defined as a dispersion of gas bubbles in liquid (Bikerman, 1973). The foam morphology in porous medium is quite different than in bulk. In porous media, foam is a dispersion of gas in a continuous liquid phase with at least some gas flow paths made discontinuous by thin liquid films called lamellae (Hirasaki, 1989). These lamellas are typically stabilized by surfactants which are adsorbed at the interface. However, lamellas lack long-term stability. In porous media, continuous regeneration of these lamellas is an essential mechanism for foam transport (Rossen, 1996). The economics of surfactant-stabilized foam depends on the quantity of surfactant required for the long distance propagation of foam from the wellbore. Various factors like surface adsorption, cost, surfactant loss due to partitioning into crude oil, and surfactant degradation under harsh reservoir conditions further limit the economic viability of surfactant usage in subsurface applications (Grigg and Mikhalin, 2007).

The use of nanoparticle can help mitigate these issues. Nanoparticles, being solid and chemically robust, can stabilize foam under harsh conditions of temperature and salinity. Moreover, these nanoparticles can be obtained cost effectively from cheap raw materials like fly ash, silica etc (Paul et al. 2007). Many studies have reported use of colloidal particles with different surface chemistry as sole stabilizers for bulk foam (Alargova et al., 2004; Binks and Horozov, 2005; Gonzenbach et al., 2006). Most of these particles were coated with surfactants or polymers to act as surface-active agents as they were not amphiphilic by themselves. Alargova et al. (2004) achieved super-stabilized aqueous foams using synthesized polymer microrods in the absence of surfactants. These foam bubbles were sterically stabilized by entangled rods-shape structures of the polymer. Binks and Horozov (2005) reported aqueous foams stabilized solely by silica nanoparticles with different degree of hydrophobicity. These stable foams were formed by adsorption of aggregates at the surfaces. Another way to obtain surface active particles is adsorption of amphiphiles on the particle surface. Gonzenbach and co-workers (2006) employed this technique to generate stable macroscopic foams. The unique colloidal architecture, i.e., the sequential assembly of amphiphiles on the surface of the particle and particle to the air-water interface, was the proposed mechanism for long-term stability of foam.

Espinosa et al. (2010) have investigated the supercritical CO_2-in-water (C/W) foam generation in beadpacks using hydrophilic silica nanoparticles coated with polyethylene glycol (PEG). The generated foam using nanoparticles dispersion had two to eighteen times more resistance to flow than the same fluid without nanoparticle. Yu et al. (2012) studied the effects of CO_2-nanoparticle dispersion phase ratio and total flow rate on CO_2 foam mobility (ratio of core effective permeability and foam viscosity) in beadpacks. The nanoparticle-stabilized foam mobility increased with increase in both dispersion phase ratio and total flow rate. Mo et al. (2012) continued this study to understand the CO_2 foam behavior in Berea sandstone cores. They reported foam generation with nanoparticle concentration as low as 100 ppm. Foam mobility attained minima when foam quality was between 40% and 80%. Aroonsri et al. (2013) investigated C/W foam generation through beadpacks, fractured and unfractured sanstones cores using various silica nanoparticles. They emphasized the role of proper hydrophilic-CO_2-philic balance (HCB) of nanoparticle selection for viscous C/W foam generation. Foam flow experiments in cores showed that a critical shear rate exists for foam generation. Worthen et al. (2012) demonstrated viscous C/W foams generation in beadpacks using partially hydrophobic silica nanoparticles which were more stable than the foam generated using hydrophilic PEG-coated silica nanoparticles.

Surface-modification of nanoparticles via chemical treatment could sometimes be expensive. In such cases, altering the surface property of particles by in situ physio-adsorption of surfactants on their surfaces could be cost effective. Several researchers have investigated the potential of utilizing this synergism between surfactant and nanoparticles to generate foam (Zhang and Somasundaran, 2006; Zhang et al., 2008; Liu et al., 2010; Cui et al., 2010). Zhang et al. (2008) demonstrated the synergistic stabilization of aqueous foams by mixtures of hydrophilic Laponite particle and non-ionic surfactant, tetraethylene glycol monododecyl ether at high surfactant concentrations. Adsorption of modified particles on air-water interface was confirmed by laser-induced confocal microscopy. Cui et al. (2010) showed that non-surface active $CaCO_3$ nanoparticles can be surface activated via interaction with anionic surfactants leading to enhanced foamability. Recently, Worthen et al. (2013) reported fine textured C/W foam generation in beadpacks using synergistic interaction of hydrophilic silica nanoparticles and surfactant, caprylamidopropyl betaine, when neither of these species could stabilize foam independently.

The interactions of surfactant and nanoparticles and their effect on foam transport in porous media are not well understood. The objective of this paper is to systematically study synergistic stabilization of foam by mixtures of surface-modified nanoparticles and anionic surfactants in bulk and porous media with and without the presence of crude oil. Foam sensitivity to various crude oils was studied and was correlated to parameters like lamella number, spreading, entering and bridging coefficients. Vertical foam films tests were done using fluorescently tagged-nanoparticles to study the foam drainage behavior. The mechanism of foam stability was analyzed in terms of detachment energy, maximum capillary pressure of coalescence, and stratification. Foams were created in-situ by co-injecting surfactant-nanoparticle mixtures and nitrogen gas through a Berea sandstone at a fixed quality and mobility reduction factors were measured. Water floods and subsequent foam floods were conducted in Berea cores saturated with a crude oil using surfactant or surfactant-nanoparticle mixture as foaming agents. The methodology and results are described in the following sections.

Methodology

Materials

Anionic surfactant Bioterge AS-40, a C_{14-16} alpha-olefin sulfonate, (39% active) was obtained from Stepan Co. The nanoparticles used in this study were aqueous dispersions of silica nanoparticles, Nyacol DP 9711, as provided by Nyacol Nano Technologies, Inc. These nanoparticles are coated with a proprietary coating (possibly polyethylene glycol, PEG) which makes them hydrophilic in nature. The size of the nanoparticles was characterized using a Transmission Electron Microscope (TEM). A FEI Tecnai TEM operating at 80kV was used. The mean diameters of primary particles were found out to be 20 nm. The TEM image is shown in Figure 1. Fluorescent silica nanoparticles, obtained from 3M, were used for fluorescence microscopy. These primary silica particles were 5 nm in diameter and PEG coating brings the particles to a

nominal diameter of 10 nm. Ultra pure water with resistivity greater than 18.2 megaohm-cm was used to prepare brine solutions. Berea sandstone cores were used in foam flow and core flood experiments. The core properties are tabulated in Table 1. Crude oils (A, B and C) were obtained from a reservoir and they had a viscosity of 9 cp, 382 cp and 36.2 cp at 25 ºC. Sodium Chloride (99%, Fisher Chemical), Nitrogen (research grade, Matheson, USA) were used as received.

Table 1. Properties of cores used

Experiments	Length	Diameter	Porosity	Permeability
Foam flow	29.36 cm	2.52 cm	23.5 %	357 mD
Coreflood-1	30.30 cm	2.47 cm	21.3 %	383 mD
Coreflood-2	30.30 cm	2.49 cm	22.9 %	315 mD

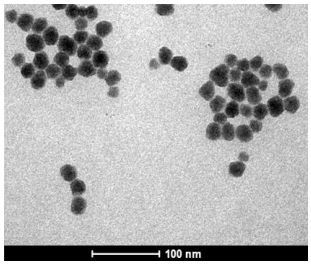

Figure 1. TEM image of surface modified-silica nanoparticles (Scale Bar is 100nm)

Preparation of Nanoparticles Dispersion

The stock solution of 1 wt% Bioterge AS-40 surfactant was prepared using ultra pure water. Samples were prepared by diluting this stock solution. Aqueous dispersion samples were prepared by incorporating silica nanoparticles with varying concentrations of 0, 0.1, 0.3, and 0.5 wt%, each having 0.5 wt% surfactant and 1 wt% sodium chloride. The dispersion was stirred for 12 hr to ensure mixture homogeneity. The particle hydrodynamic diameters in the aqueous dispersions were characterized using the Delsa™ Nano analyzer.

Foamability and Static Foam Tests

Preliminary foam tests were conducted by shaking 5 ml of these samples vigorously for 10 times in test tubes and the macroscopic foam textures were observed. In case of foam shake tests in presence of crude oil, 10 wt% of oil was initially added to samples before vigorous mixing. 100 ml of each sample was then taken in a graduated glass cylinder (diameter: 4 cm, length: 30 cm) at room temperature. Air was injected from the bottom and static foam was generated. The cylinder was always sealed from the top using a rubber cork. The height of the foam (above the liquid phase) was monitored as the time progressed. In foam tests in the presence of crude oils, first the foam was generated by dispersing the air and then oil (2 wt %) was introduced from the bottom using a very fine tube. A different setup was used to conduct these experiments at higher temperatures. The apparatus consisted of a transparent cylinder made of acrylic with a stainless steel hollow needle at the bottom which was used to inject air. Both ends of the cylinder had Swagelok fittings which prevented evaporation. The experiments were conducted at several temperatures (55 ºC, 75 ºC, and 95 ºC) by placing the setup in an oven. In each experiment, 20 ml solution was taken in the cylinder and was kept in oven for sufficient time to attain equilibrium temperature and then foam was generated.

Vertical Foam Film Tests

The foam drainage behavior was visualized by making foam in a small, vertically-oriented, optical glass cell (4 x 12 x 48 mm; Produstrial, Fredon, NJ). Small amount of nanoparticle dispersion to be studied (0.5 ml) was taken in the cell and foam was generated by dispersing air from the bottom using a syringe. The time-dependent foam morphology was observed using a Nikon microscope equipped with a high resolution camera. Images were recorded every 30 seconds using Image Pro software and lamella width was measured after sufficient drainage time. Similar experiments were conducted using the dispersion of fluorescently tagged-nanoparticles. Images of foam texture was captured both in visible as well as UV light. All these measurements were done at the ambient temperature.

Foam Flow Experiments

The cores were dried at 90 ºC for 24 hours in an oven and were laminated with FEP shrink wrap tubing (Geophysical Supply Company, Houston, TX). These were then placed in a Hassler-type core holder (Phoenix, Houston, TX) with a confining pressure of 1500 psi. The air porosity and permeability of the cores were then determined. Figure 2 shows the experimental schematic. Two Series-D syringe pumps from Teledyne ISCO (Lincoln, NE) were used in the setup which are capable of low injection rates (as low as 0.001cc/min). The apparatus was built to co-inject nitrogen gas and surfactant or surfactant-NP blends through a sandpack (0.6 inch diameter and 6 inch long) to ensure proper mixing and foam generation. The pre-generated foam was then injected from the top of the core in the core holder. The effluent from the core went to a high pressure view cell. The downstream pressure of the experiment was maintained by a back pressure regulator (Equilibar, NC) installed after the view cell. The pressure drops across various sections of core were measured using Rosemount differential pressure transducers. All connections were made with stainless steel Swagelok fittings.

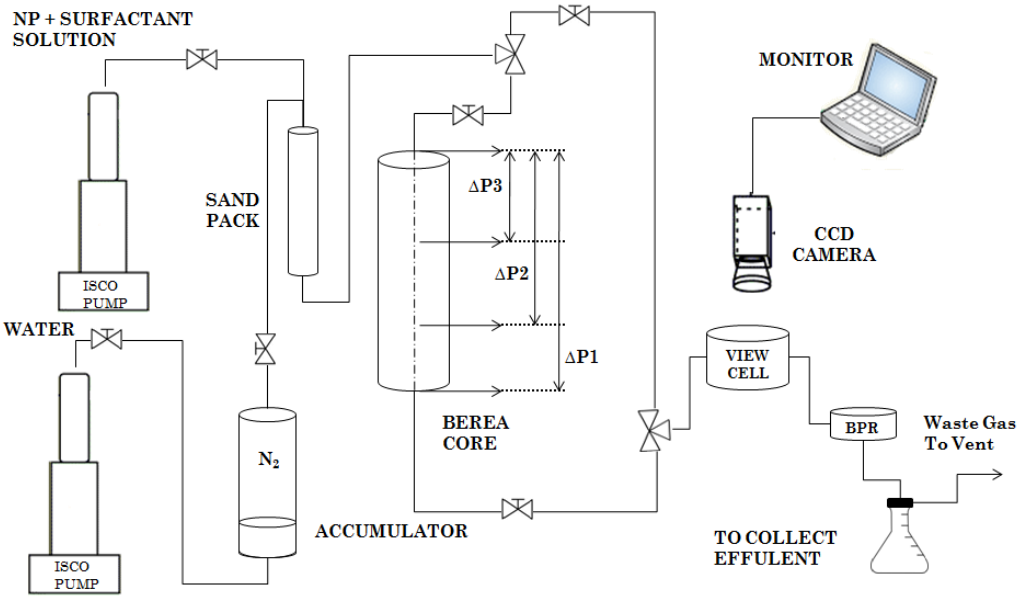

Figure 2. Schematic of the apparatus for foam flow experiments and corefloods

Oil Displacement Experiments

The experimental setup was similar to Figure 2 except the view cell was removed to lower the dead volume of the setup to accurately measure the oil recovery. The brine porosity and permeability of the cores were determined. The cores, fully saturated with brine, were then flooded with filtered crude oil (at least 2.5PV) from the top at a constant pressure of 750 psi at room temperature until no brine was produced. The initial oil saturation was determined by mass balance. The whole setup was pressurized with a back pressure of 100 psi. The brine flood was conducted at 1ft/day for 2 PV until no oil was produced. Then, it was flooded with brine at 5 ft/day to minimize capillary end effects. The cores were then pre-flushed with 1 PV of surfactant or surfactant-NP blend to avoid any adsorption of surfactant while foam flooding. Nitrogen gas and surfactant or surfactant-NP blend were then co-injected through sand pack to make foam. This pregenerated foam was then injected into the core from the top for more than 7 PV. Oil recovery and pressure drops were monitored at each step.

Results and Discussion

Foamability and Foam Sensitivity to Crude Oil

Basic shake test was performed using 0.5 wt% of surfactant in 1 wt% sodium chloride with varying nanoparticle concentrations from 0 to 0.5 wt%. The foam drainage behavior was not studied in these experiments and only the macroscopic foam behavior was observed. The results (Figure 3) show that these samples have good foaming tendency in the absence of oil. No significant differences were observed (by naked eyes) in the macroscopic foam texture with increasing nanoparticles concentration in the solution. This experiment was then repeated in the presence of crude oil. Before mixing the solution, 10 wt% crude oil was added to the solution. Three crude oils (A, B and C) were used in this test; they had a viscosity of 9 cp, 382 cp and 36.2 cp, respectively. Figure 4 shows the foam morphology at time, t=0 min formed using 0.5 wt% of surfactant solution in the presence of these crude oils.

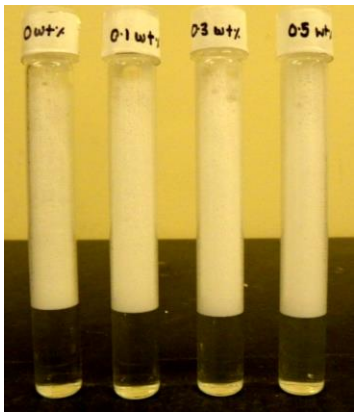

Figure 3. Foam morphology with 0.5 wt% surfactant at 0, 0.1, 0.3, and 0.5 wt% nanoparticle concentrations (from left to right)

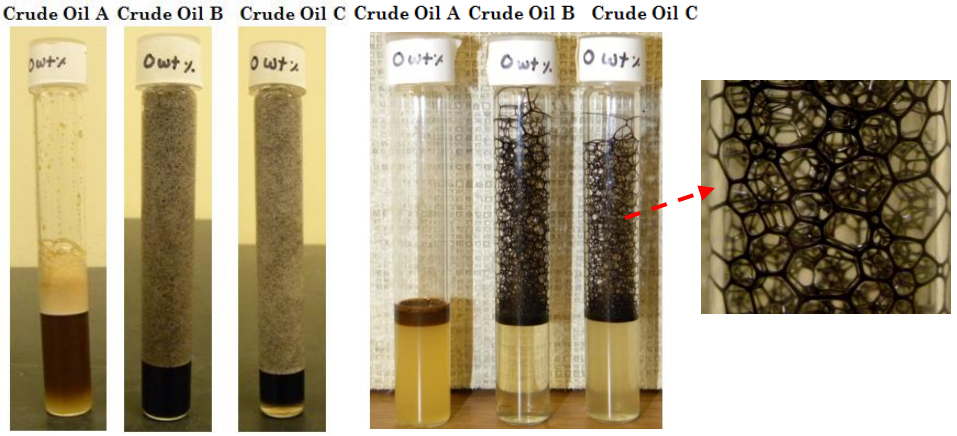

Figure 4. Foam morphology with 0.5 wt% surfactant in the presence of oil at time (a) t=0 minute (left); (b) t=8 hr (right)

It was seen that foam volume decreased drastically for the case of crude oil A indicating that foam was not stable with this crude oil. Oil was instantaneously drained to the bulk solution rupturing the foam lamellas showing no retention ability of oil within a lamella. For the case of crude oil B and C, foam volume was retained at the maximum at time, t=0 minutes and even for longer duration (> 8hr) as shown in Figure 4. In both of these samples, oil was seen distinctly inside the foam lamellas indicating the tendency of oil to imbibe into the lamella without rupturing it. Thus, the foam was quite stable even in the presence of crude oil B and C. This test was repeated with samples having 0.5wt% surfactant and 0.3 wt% nanoparticles and the same macroscopic foam behavior was observed.

It can be seen that foam behaves differently with different crude oils. Typically, oils are known to be detrimental to foam stability and generally considered as foam inhibiting or antifoaming agents (Denkov, 2004). Many researchers have reported this destabilizing effect of oil on foam stability in porous media (Irani and Solomon, 1986; Kuhlman, 1990; Jensen and Friedmann, 1987). Understanding the phenomenon of foam-oil interactions are quite complex, however a qualitative analysis can be done by investigating several parameters which are dependent on surface energies of the system. Spreading coefficients (Eq. 1), entering coefficients (Eq. 2) and bridging coefficients (Eq. 3) are three such parameters, defined as follows:

$$S = \sigma_{w/g} - \sigma_{w/o} - \sigma_{o/g} \quad [1]$$

$$E = \sigma_{w/g} + \sigma_{w/o} - \sigma_{o/g} \quad [2]$$

$$B = \sigma_{w/g}^{\ 2} + \sigma_{w/o}^{\ 2} - \sigma_{o/g}^{\ 2} \quad [3]$$

where σ is the interfacial tension and the subscripts w, g, and o correspond to water, gas and oil, respectively. From thermodynamics, a negative value of spreading coefficient, S implies that foam will be stable in the presence of oil (Harkins, 1941). Similarly, the foam-oil system is stable when entering coefficient, E is negative (Robinson and Woods, 1948). A positive value of bridging coefficient, B is a necessary (not sufficient) condition for the oil to act as antifoaming agent (Denkov, 2004). Schramm and Novosad (1990) have suggested the parameter lamella number, L, i.e.,

$$L = 0.15 * \frac{\sigma_{w/g}}{\sigma_{w/o}} \quad [4]$$

to indicate whether oil can imbibe into foam lamellas. Based on the value of this number, the foam was classified into three types. L< 1, 1< L < 7 and L > 7 corresponds to Type A, B and C, respectively. Type A foams represent the most stable foams which do not interact with oil. They have both negative E and S. Type B foams have negative S and positive E and are moderately stable. They interact with foam lamellas, but do not rupture them. Type C foams are unstable foam with both positive S and E. Oil tends to imbibe in these foams and ruptures the foam lamellas.

Table 2 shows the measured interfacial surface tensions of oil-gas-surfactant systems for the three crude oils. The presence of nanoparticles (used in this study) did not alter the surface tension values significantly, so the values of the parameters S, E, L and B would be the same for the case of the oil-gas-surfactant-NP system. Figure 4 shows the foam texture after 8 hours. It can be seen that foams were not stable with crude oil A (μ = 9cp) and were quite stable with crude oils B (μ = 382 cp) and C (μ = 36.2 cp). Thus, foam sensitivity to crude oil analysis revealed that lighter crude oils are more destabilizing to foams than heavier oils. The calculated values of spreading coefficients, entering coefficients, lamella number, and bridging coefficients are listed in Table 3. Results show that spreading coefficients, entering coefficients and bridging coefficient are positive for all the three crude oil systems. Thus, these parameters were not reliable in predicting the stability of the foam-oil system. Lamella number predicted crude oil system A to be of type C and crude oils B and C to be of type B, which is consistent with the macroscopic observation of these foams. However, by definition of Type B foam, spreading coefficient should be negative which was not the case.

Table 2. Interfacial tension data for the three oil

System	Interfacial Tension (mN/m)		
	Oil A	Oil B	Oil C
Oil-Gas	21.31	22.16	20.73
Oil-Surfactant	0.08	4.03	2.35
Air-Surfactant	31.69	31.69	31.69

Table 3. Calculated parameters based on interfacial data

Parameters	Oil A	Oil B	Oil C
Spreading Coefficient (S)	10.3	5.4	8.61
Entering Coefficient (E)	10.4	13.5	13.31
Lamella Number (L)	59.4	1.2	2.02

Static Foam Tests

Static foam tests were carried out with nanoparticles dispersed in 0.5 wt% of surfactant with varying concentrations from 0.1 wt% to 0.5 wt% and foamability was compared with that of 0.5 wt% of surfactant alone. The decay of foam height was monitored with time. These experiments were conducted at the room temperature. The results are plotted in Figure 5. Half-life, which is the time it takes for the foam to decay to half of its original height, can be seen from the plot. Half-life of foams generated using surfactants alone without nanoparticles was about 48 hr. As the concentration of nanoparticles was increased to 0.1 wt%, the foamability of solution improved and half-life increased to 68 hr. The synergistic effects on foaming of surfactant-nanoparticle system became more pronounced when nanoparticles concentration was increased to more than 0.3 wt%. The foam heights almost remained almost constant for days (>4 days). The mechanisms behind this synergy and enhanced bulk foam stability by combination of surfactant and nanoparticles are studied in the subsequent sections.

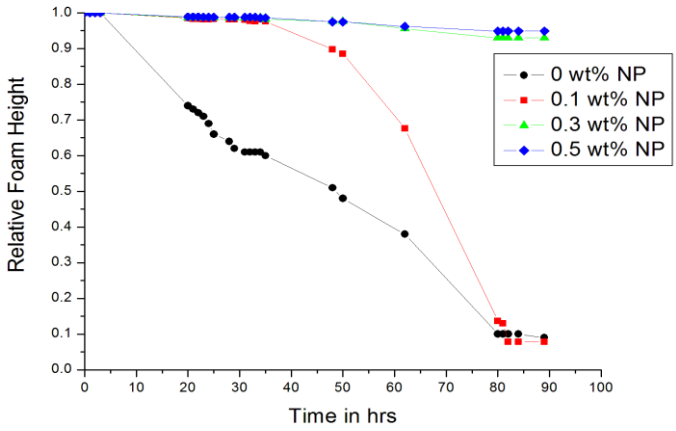

Figure 5. Static foam tests with 0.5 wt% surfactant and varying nanoparticle concentration at 25 ºC

These foam tests were then repeated in the presence the crude oil A, B, and C using 0.5 wt% surfactant with and without nanoparticles at the room temperature. The nanoparticles concentration used in these cases were 0.3 wt%. Foams were first generated and then 10 wt% of crude oil was introduced from the bottom using a fine tube. The macroscopic foam-oil interactions and foam height was observed with time. Figure 6 shows the foam height decay profile in the presence of crude oil A as well as foam-oil interaction at the oil interface. The image was captured just after the introduction of oil to the foam system. As seen in the preliminary foam tests, crude oil A was quite detrimental to foam. As soon as the oil came in contact with the foam, it resulted in rupturing of the lamellas which cause rapid decay of foam with time. The half-life in this case was only 24 minutes for both surfactant and surfactant-NP blend. No additional stabilization of foam was observed due to presence of nanoparticles as the deleterious effect of oil on foam dominated the foam decay. The half-life in the absence of crude oil was of the order of days and in presence of crude oil A, it is only of the order of minutes. In case of crude oils, B and C, there was no detrimental effect on the foam when they were introduced beneath the foam. The oil did not rupture the lamellas on contact that resulted in longer half-lives. The additional stability of foam was observed in surfactant-nanoparticle blends as compared to surfactant alone as evident from longer half-lives. The half-lives increased from 12 hr to 22 hr for the case of crude oil B and it increased from 10 hr to 14 hr for the case of crude oil C (Figure 7).

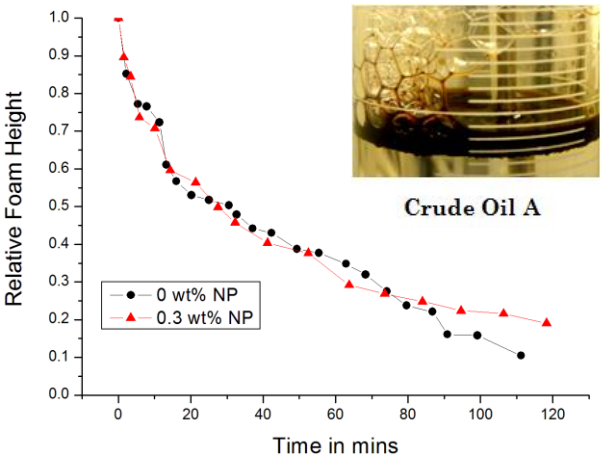

Figure 6. Static foam tests with crude oil A at 25 ºC

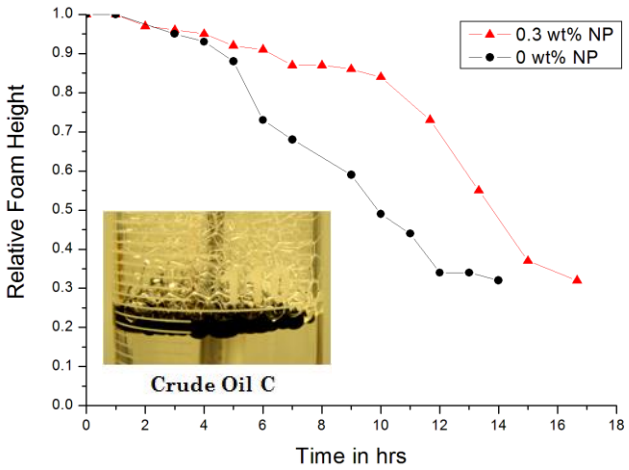

Figure 7. Static foam tests with crude oil C at 25 ºC

A series of static foam tests were then conducted at higher temperatures (95 ºC, 75 ºC, 55 ºC) to compare the foamabilty of 0.5 wt% of surfactant with and without nanoparticles in the absence of crude oil. The objective was to investigate the synergy of nanoparticles-surfactant system at harsh conditions, since most of the subsurface processes are at elevated temperatures. The nanoparticles concentration was kept 0.3 wt% as in earlier tests. Since these tests were performed at higher temperature, evaporation effects were needed to be minimized. So, a different setup was used to do these experiments which can provide leak-proof connections. As the dimensions of the cylinder, needle's diameter of the air disperser and amount of liquid initially taken were different as compared to previous setup, the results of these tests should not be compared with results from first setup for analysis. The results showed that foam decayed at much faster rate at higher temperatures than room temperature because of the viscosity reduction of the bulk solution. However, it was observed that with the presence of nanoparticles, half-lives of foam were increased considerably for each temperature case. For the surfactant, the half-lives were 2 minutes, 5 minutes, and 50 minutes and for the surfactant-nanoparticles blend they were 16 minutes, 36 minutes, and >450 minutes at 95 º C, 75 º C, and 55 º C, respectively. This implies that nanoparticles have the ability to impart strength to the foam structure making it less susceptible to temperature increase.

Vertical Foam Films Tests

Foam was generated in the optical glass cell using 0.5 wt % surfactant solution with and without nanoparticles. The concentration of nanoparticles in the former case was 0.3 wt%. The bubbles were formed between the parallel walls of foam cells spanning both sides. The typical bubble structure can be considered as polygonal prism and is shown in Figure 8. A Gibbs-Plateau border is formed when three neighboring bubbles meet at one edge. The foam morphology was observed using high-resolution microscope. After allowing sufficient drainage time of 30 minutes, the images of foam were captured. Figure 8 shows the foam structure for surfactant and surfactant-NP blend, respectively. The typical lamella width in surfactant case was found out to be about 340 microns, while for the blend it was 472 microns. The experiment was repeated several times to check for reproducibility and results were consistent with a variation of ± 20 microns. The thicker lamella width for the surfactant-NP blend case indicates retarded drainage process.

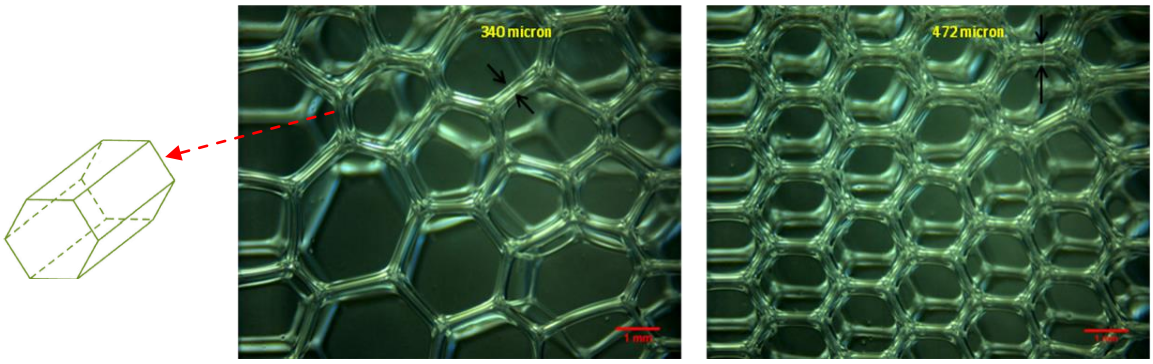

Figure 8. Vertical foam films made using (a) 0.5wt% surfactant (left) and (b) 0.5wt% surfactant and 0.3wt% NP (right)

To fundamentally understand the mechanism of enhanced foam stability and thicker lamella width for the case of surfactant-NP blend, fluorescently-tagged nanoparticles (FL-NP) were used. Foam was generated using 0.5 wt% surfactant with 0.3 wt% FL-NP in the foam cell. The foam drainage behavior was observed using a vertical-stage microscope. Figure 9 shows the foam structure after 30 minutes of drainage in visible light and in UV light. From the front view of vertical films, the cross-section of the horizontal plateau border which is perpendicular to the foam cell can be seen. The locations of the nanoparticles, i.e., fluorescence, can be easily seen from the image captured in the UV light. Most of nanoparticles are trapped in the Gibbs-Plateau border and the lamellas in between the bubbles and they present a physical barrier in the drainage of free liquid and retard the coalescence process. To confirm these observations, confocal laser scanning microscopy (CLSM) testing was done using the same FL-NP. Fluorescent nanoparticles could be seen surrounding the bubbles and dispersed in the continuous liquid phase. These nanoparticles in bulk form three-dimensional networks that enhance the stability of the bubbles.

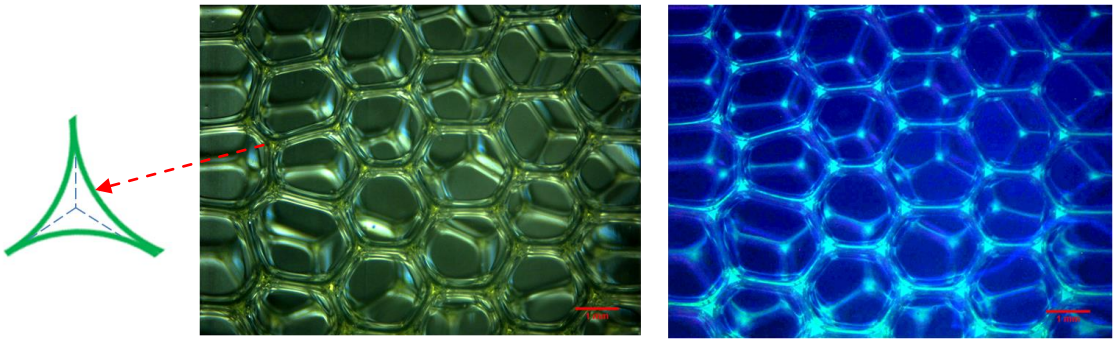

Figure 9. Vertical foam films made using FL-NP; Image captured in (a) visible light (b) UV light

Mechanisms for Foam Stability in Bulk

Synergistic stabilization of foams by surfactant-nanoparticle systems depends on the interplay of nanoparticle-interface, surfactant-interface and nanoparticle-surfactant interactions. Some of the key mechanisms presented in literature for particle stabilized foams have been analyzed here for surfactant-nanoparticle systems.

Particle Detachment Energy

The energy required to detach a particle of radius R from the interface depends on the contact angle θ and surface tension γ_{aw} of the interface (Binks and Lumsdon, 2000). If the particle size is quite small (< few microns), gravity and buoyancy effects can be neglected. The amount of energy required to move the particle from the interface to the bulk solution is given by:

$$E = \pi R^2 \gamma_{aw} (1 - |\cos\theta|)^2 \quad [5]$$

For contact angle, θ < 30º (highly hydrophilic particle) or θ > 150º (highly hydrophobic particle), this detachment energy would be quite low which implies that the particle cannot stabilize foam (as per this theory). For a contact angle close to 90º and a particle of diameter 10 nm, this detachment energy is quite large (in the absence of surfactants) and it is of the order of 10^3 kT. The large energy associated with attachment implies that once the nanoparticle is brought to the interface, it would be irreversibly adsorbed on the interface and will provide robust foam stability (Binks, 2002). Nyacol's NP coated with a proprietary coating (20 nm) and 3M's FL-NP coated with PEG (10 nm) are one order of magnitude larger than a typical surfactant which implies large adsorption energy. The presence of surfactant reduces this energy by about half because the surface tension decreases from about 70 dyne/cm to about 30 dyne/cm. This hypothesis suggests that highly hydrophilic particles do not stabilize interfaces, but they can by other mechanisms, as discussed below.

Maximum Capillary Pressure of Coalescence

In the absence of nanoparticles, the foam films are flat and the capillary pressure P_c is balanced by the disjoining pressure in the foam film. When the capillary pressure exceeds a threshold pressure, P_c^{max} the film ruptures (Denkov et al. 1992). In the presence of nanoparticles, the films do not have to be flat. Nanoparticles have the potential to provide a steric barrier in the thinning of foam films and thus play a major role in retarding coalescence of foam bubbles. Kaptay (2006) has derived an expression for the maximum capillary pressure by analyzing a single hexagonal layer of particles between two bubble films, i.e.,

$$P_c^{max} = \beta \frac{2\gamma_{aw}}{R} \cos\theta \quad [6]$$

where β is a theoretical packing parameter, γ_{aw} is the air-water interfacial tension and R is the particle radius. As the radius decreases, the maximum capillary pressure the film can experience without rupturing increases. This is how nanoparticles can stabilize films. Figure 10 shows a spherical particle that bridge between two bubble films with contact angle θ. If this angle is > 90º, the positive capillary pressure in the film adjacent to the particles will cause drainage of liquid away from particle which will cause the dewetting of the films and formation of a hole (Figure 10a). However, for contact angle < 90º, as in the present case of hydrophilic nanoparticles, after an initial drainage; a critical film thickness is achieved and the film gets planar. Further drainage causes the capillary pressure to draw liquid towards the particle and thus stabilizing the film by bridging mechanism (Figure 10b) (Pugh, 1996). This theory explains how foam films can be stabilized by bridging hydrophilic nanoparticles.

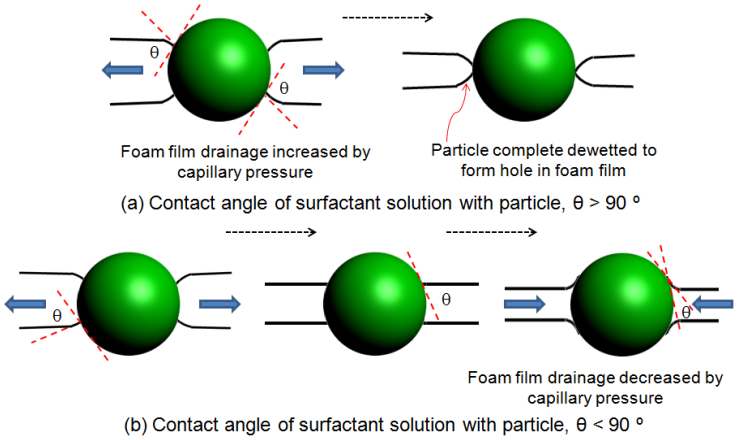

Figure 10. Bridging particle behavior in a foam (a) hydrophobic (b) hydrophilic particles (adapted from Aveyard et al., 1994)

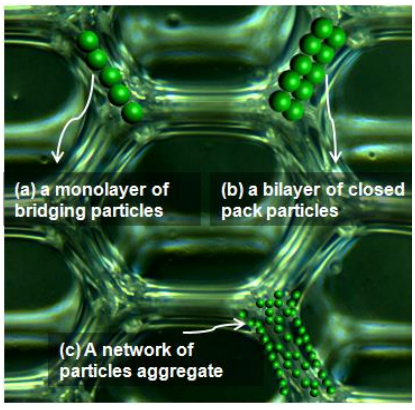

Figure 11. Three possible mechanism of liquid film stabilization (adapted from Horozov, 2008)

Kinetics of Film Drainage

Horozov (2008) has suggested three possible ways hydrophilic particles can be incorporated inside liquid films: (a) a monolayer of bridging particles, (b) a bilayer of closed-pack particles, and (c) a network of particle aggregates inside the film. Figure 11 illustrates these three cases in foam films. The images of the vertical foam films using FL-NP suggest that some of the nanoparticles drain into the plateau borders from foam films. The particles (surfactant molecules or nanoparticles) are forced to attain an orderly arrangement within a thinning inter-bubble film, resulting in stepwise thinning of the film. This stratification process slows down liquid drainage and provides additional foam stability in conjunction with the disjoining pressure. The driving force for the particle exhibiting stepwise thinning is the chemical potential gradient of particle at film periphery, where particle leaves the interface and a vacancy is formed at its place (Kralchevsky et al., 1990). Johonnott (1906) was first to show these behavior in foam film studies using surfactants at high concentrations. Sethumadhavan et al. (2001, 2004) reported the stratification behavior of silica nanoparticles resulting in film stability. This tendency of orderly arrangement of particles was reported to decrease significantly as the polydispersivity of the solution was increased. Nanoparticles used in the present study are highly monodisperse with very low polydispersity index which suggests slow drainage of films.

Foam Flow Experiments

Foam flow experiments were conducted in 1-ft long Berea sandstone cores using 0.5 wt% surfactant with varying nanoparticle concentrations from 0.1 wt% to 0.5 wt% as foaming agents. The pressure drop profiles across the different sections of the cores were monitored. The macroscopic foam texture of effluent coming out of the core was visualized using the view-cell installed at the downstream end of the core. The flow rates in these experiments were kept at 4 ft/day. This was done to get a large enough pressure drop which can be measured accurately. All these experiments were performed at the room temperature and with a back pressure of 100 psi.

First, the surfactant pre-flush was conducted to saturate the core with surfactant and avoid any surfactant adsorption issues while foam flooding. Steady state pressure drop was measured after 3 PV of injection which was very low (about 0.1 psi). After the surfactant pre-flush, nitrogen gas and surfactant solution (without nanoparticles) were co-injected into the sandpack to generate foam at 4 ft/day and with a quality of 80%. This pre-generated foam was injected from the top of the core for at least 5 PV to achieve a steady state pressure drop. Figure 12 shows the pressure drop obtained for this case and high-pressure foam texture as seen in the view cell after the steady state. The pressure drop has many fluctuations, but the average pressure drop in the steady state was about 9.7 psi. The average bubble diameter, measured from the foam texture, was about 910 microns.

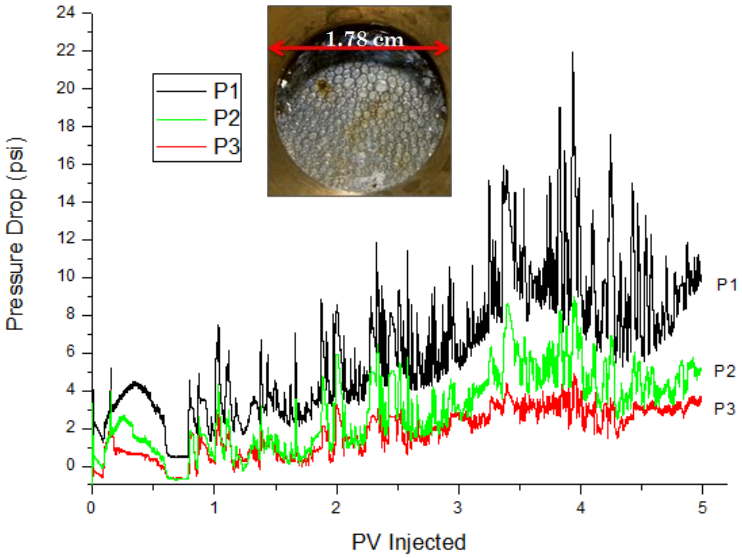

Figure 12. Pressure drop profile for the co-injection of nitrogen and surfactant at 4ft/day with quality of 80%

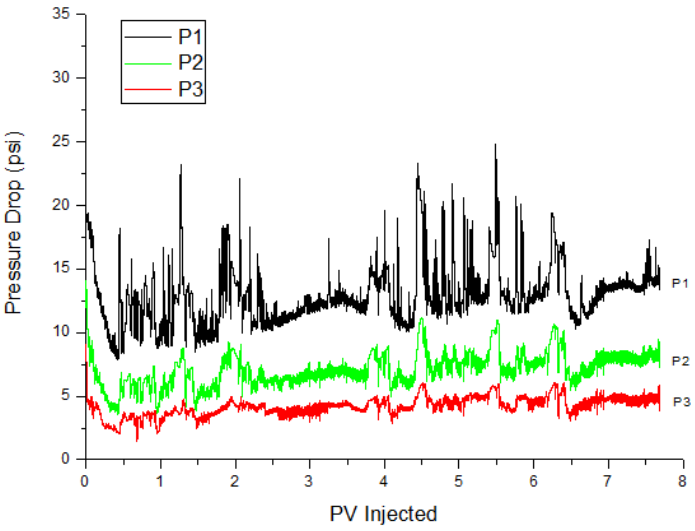

Figure 13. Pressure drop profile for the co-injection of 0.5 wt% surfactant with 0.1wt% nanoparticle at 4ft/day with quality of 80%

In the subsequent steps, nanoparticles concentration was varied from 0.1 wt% to 0.5 wt% in the injection fluid keeping the same surfactant concentration (0.5 wt%). Flow rate was kept at 4 ft/day with 80% quality throughout the experiment. Steady state pressure drops were typically achieved after 8 PV of co-injection. Figure 13 shows the pressure drop profile when 0.1 wt% of nanoparticles was used. The average steady state pressure drop was about 13.74 psi which is slightly more than the case with no nanoparticles which indicates a stronger foam. Then nanoparticle concentration was raised to 0.3 wt% in the injection fluid. Figure 14 shows the pressure drop profile and the steady state foam texture. Steady state pressure drop in this case was 17.43 psi. It can be seen that macroscopic foam texture in this case is quite dense characterized by fine textured

bubbles. The average bubble diameter was found to be 330 micron which is smaller than those for the only surfactant case. Large pressure drop achieved in this case is due to finer in-situ bubble texture stabilized by surfactant-nanoparticle system. With 0.5 wt% concentration of NP, the steady-state pressure increased to 21.47 psi.

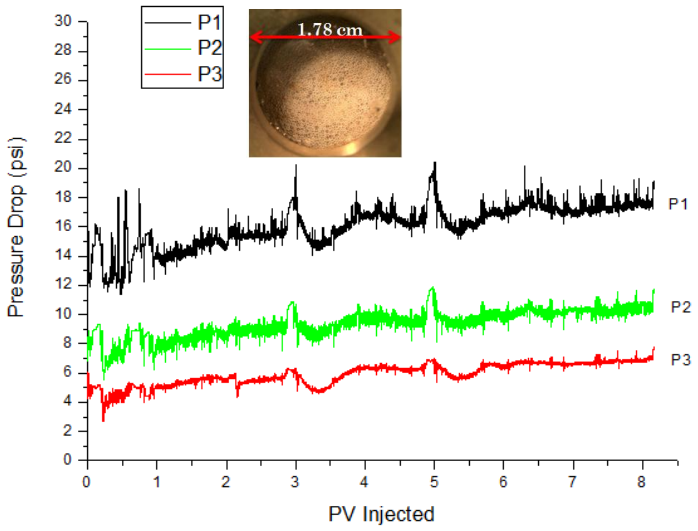

Figure 14. Pressure drop profile for the co-injection of 0.5 wt% surfactant with 0.3wt% nanoparticle at 4ft/day with quality of 80%

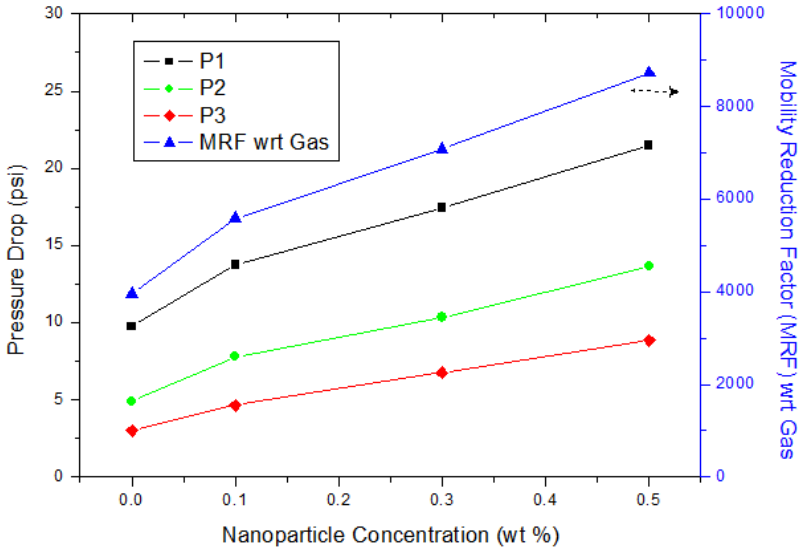

Figure 15. Steady state pressure drops (left axis) and mobility reduction factors (right axis) achieved using varying concentration of nanoparticles

Mobility reduction factor (MRF) is defined (here) as the ratio of the pressure drop across the core due to foam flow and the pressure drop due to single phase gas flow at the same flow rate. Figure 15 is the plot of steady state pressure drops and mobility reduction factors achieved for varying concentration of nanoparticles. As the nanoparticle concentration increases from 0 wt% to 0.5 wt%, the MRF increases from 4000 to 8700.

Oil Displacement Experiments

Core flood 1 was conducted in a Berea core with a reservoir dead crude oil C. The initial oil saturation was 64 %. Figure 16 shows the injection procedure, cumulative oil recovery and overall pressure drop across the core. Brine flood was conducted at 1 ft/day to mimic the waterflood at a typical field rate. It was continued for 2 PV until no oil was produced. The waterflood oil recovery was 54.4 %OOIP (original oil in place) and oil saturation was reduced to 29.2 %. The pressure drop during water flood was between 1-3 psi. Then, brine was injected at 5 ft/day for another 1 PV to minimize any capillary end effect issues. The pressure drop increased to 7.4 psi as the flow rate was increased 5 times. No oil was recovered during this stage implying no significant capillary end effects. Before conducting the foam flood, the core was pre-flushed with 0.5 wt% surfactant for 1 PV at 1 ft/day to avoid any surfactant adsorption during foam flooding. No oil was recovered during surfactant injection as the surfactant does not lower the IFT sufficiently to mobilize residual oil. The pressure drop during pre-flush was almost constant at 1.1 psi. Then, co-injection of 0.5 wt% of surfactant solution and nitrogen gas was started with a quality of 80% at 1ft/day. Since there is some dead volume before the core as explained earlier, the pressure drop increase due to in-situ foam generation was delayed by about 0.7 PV. The additional oil recovery for first 3.5 PV of co-injection over waterflood was 9.3% OOIP. No significant amount of oil was produced after 3.5 PV of injection but the co-injection was continued for another 4.5 PV to observe the foam mobility in the presence of residual oil. The average pressure drop continued to grow and reached about 9 psi at the end of experiment. The ultimate cumulative oil recovery was 63.8 %OOIP and final oil saturation was 23.2%.

The second core flood (core flood 2) was conducted in another Berea core with the same procedure as the previous core flood, but with surfactant and nanoparticles. The initial oil saturation in this case was 63.8%. The cumulative oil recovery (%OOIP) and overall pressure drop are shown in Figure 17. The core was flooded with brine for 2 PV at 1 ft/day which represents a water flood. The water flood reduced the oil saturation to 29.8% and resulted in 53.3 %OOIP oil recovery. The pressure drop during this stage was low (~ 2 psi). Then, the core was flooded with brine for 1 PV at 5 ft/day. No additional oil was recovered implying negligible capillary end effects. The pressure drop increased to about 10.5 psi at the flow rate of 5 ft/day. Then, the core was pre-flushed with 0.5 wt% of surfactant for 1 PV. No oil was recovered during this stage. Co-injection of 0.3 wt% nanoparticles in 0.5 wt% surfactant solution and nitrogen gas was then started at 1ft/day with 80% quality. The additional oil recovery over water flood after 3.5 PV of injection was 10.6 %OOIP. The co-injection was continued for another 4.5PV. The pressure drop in this core flood went to around 9.8 psi at the end of the experiment.

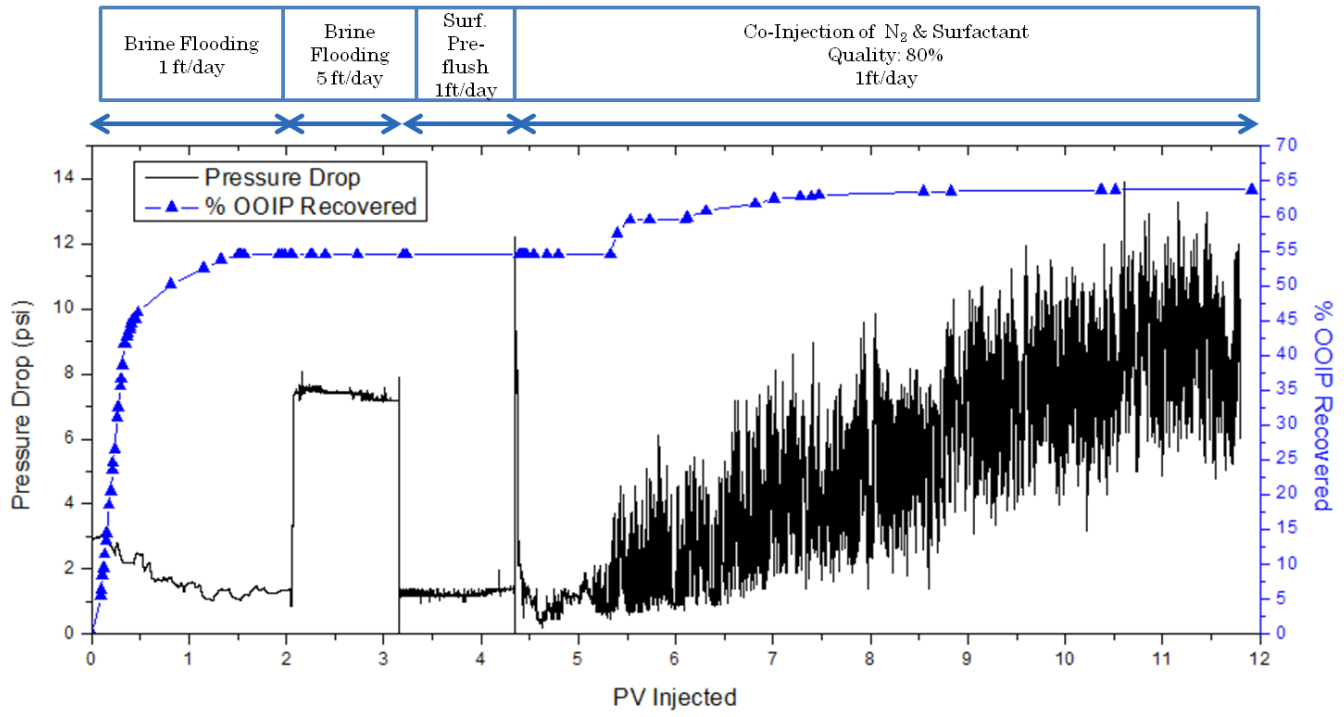

Figure 16. Pressure drop profile (left axis) and cumulative oil recovery (right axis) for the core flood 1

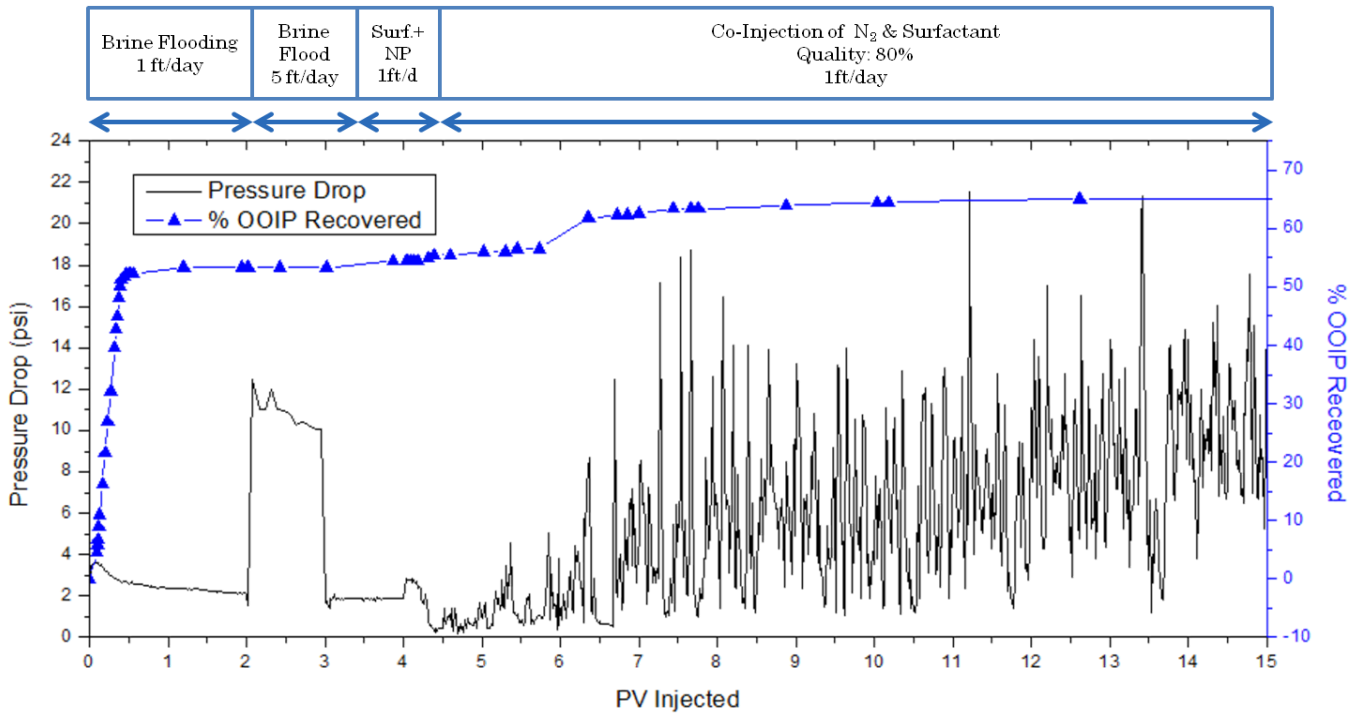

Figure 17. Pressure drop profile (left axis) and cumulative oil recovery (right axis) for the core flood 2

The objective of these oil displacement experiments in water-wet cores was to investigate the potential of immiscible foam stabilized by surfactant or surfactant-NP blend in displacing the residual oil. In water-wet systems, immiscible foam can increase the trapped gas saturation which decreases the residual oil saturation resulting in additional oil recovery. Moreover, they can reduce the gas mobility significantly. The cores used in the corefloods were only one inch in diameter and were quite homogenous, so volumetric sweep efficiency improvement was not an important factor here. The oil displacement experiments showed that the incremental oil recovery over waterflood using surfactant-nanoparticle blend (10.6 %OOIP) was slightly higher than that with the surfactant (9.3 %OOIP). Since the injected gas/foam was immiscible with the oil, the incremental oil recoveries for these 1D-corefloods were significant. Mobility reduction factor achieved in both the cases were quite similar. The effectiveness of the immiscible foams can be better tested in multi-dimensional flows and heterogeneous media.

Conclusions

The following conclusions can be drawn from this work:

- Static foam tests indicate stabilization effect of nanoparticles on surfactant-nanoparticle foam stability in the absence of crude oil. A dramatic increase in half-lives of foam was observed with increasing nanoparticle concentration.
- Vertical foam film tests elucidated that nanoparticles are trapped in the plateau border as well as lamellas which retard liquid drainage and bubble coalescence. The observation was confirmed using confocal laser scanning microscopy.
- The classification of foams based on lamella number was found to be in agreement with the macroscopic foam-oil interaction behavior. The spreading, entering, and bridging coefficients were found to be unreliable parameters to estimate foam-oil stability.
- As the concentration of nanoparticles increased, mobility reduction factor (MRF) of surfactant-nanoparticle foam in a Berea core increased significantly.
- Core flood in a sandstone core with a reservoir crude oil showed that immiscible foams using surfactant-nanoparticle blend can increase the oil recovery (over water flood) by about 10% OOIP.

Acknowledgments

We are thankful to the sponsors of Gas EOR Industrial Affiliates Project at The University of Texas at Austin for partial funding of this work. We would also like to thank Dr. Eric Dao in helping us with the experimental set-up.

References

Alargova, R. G., Warhadpande, D. S., Paunov, V. N., & Velev, O. D. (2004). Foam superstabilization by polymer microrods. *Langmuir*, *20*(24), 10371-10374.

Aroonsri, A., Worthen, A. J., Hariz, T., Huh, C., Johnston, K. P., & Bryant, S. L. (2013, September). Conditions for Generating Nanoparticle-Stabilized CO Foams in Fracture and Matrix Flow. In *SPE Annual Technical Conference and Exhibition*. Society of Petroleum Engineers.

Aveyard, R., Binks, B. P., Fletcher, P. D. I., Peck, T. G., & Rutherford, C. E. (1994). Aspects of aqueous foam stability in the presence of hydrocarbon oils and solid particles. *Advances in colloid and interface science*, *48*, 93-120.

Bikerman, J. J. (1973). *Foams* (pp. 65-97). New York: Springer-Verlag.

Binks, B. P., & Lumsdon, S. O. (2000). Influence of particle wettability on the type and stability of surfactant-free emulsions. *Langmuir*, *16*(23), 8622-8631.

Binks, B. P. (2002). Particles as surfactants—similarities and differences.*Current Opinion in Colloid & Interface Science*, *7*(1), 21-41.

Binks, B. P., & Horozov, T. S. (2005). Aqueous foams stabilized solely by silica nanoparticles. *Angewandte Chemie*, *117*(24), 3788-3791.

Bond, D.C., and Holbrook, O.C., Gas drive oil recovery process, US Patent, No. 2,866,507 (1958).

Cui, Z. G., Cui, Y. Z., Cui, C. F., Chen, Z., & Binks, B. P. (2010). Aqueous foams stabilized by in situ surface activation of CaCO3 nanoparticles via adsorption of anionic surfactant. *Langmuir*, *26*(15), 12567-12574.

Denkov, N. D., Ivanov, I. B., Kralchevsky, P. A., & Wasan, D. T. (1992). A possible mechanism of stabilization of emulsions by solid particles. *Journal of colloid and interface science*, *150*(2), 589-593.

Denkov, N. D. (2004). Mechanisms of foam destruction by oil-based antifoams.*Langmuir*, *20*(22), 9463-9505.

Dickinson, E., Ettelaie, R., Kostakis, T., & Murray, B. S. (2004). Factors controlling the formation and stability of air bubbles stabilized by partially hydrophobic silica nanoparticles. *Langmuir*, *20*(20), 8517-8525.

Enick, R., Olsen, D., Ammer, J., & Schuller, W. (2012, April). Mobility and Conformance Control for CO2 EOR via Thickeners, Foams, and Gels--A Literature Review of 40 Years of Research and Pilot Tests. In *SPE Improved Oil Recovery Symposium*.

Espinoza, D., Caldelas, F., Johnston, K., Bryant, S., & Huh, C. (2010, April). Nanoparticle-stabilized supercritical CO2 foams for potential mobility control applications. In *SPE Improved Oil Recovery Symposium*.

Gonzenbach, U. T., Studart, A. R., Tervoort, E., & Gauckler, L. J. (2006). Ultrastable Particle-Stabilized Foams. *Angewandte Chemie International Edition*, *45*(21), 3526-3530.

Grigg, R. B., & Mikhalin, A. A. (2007, January 1). Effects of Flow Conditions and Surfactant Availability on Adsorption. *Society of Petroleum Engineers*. doi:10.2118/106205-MS

Harkins, W. D. (1941). A general thermodynamic theory of the spreading of liquids to form duplex films and of liquids or solids to form monolayers. *The Journal of Chemical Physics*, *9*, 552.

Hirasaki, G. J. (1989). Supplement to SPE 19505 The Steam-Foam Process--Review of Steam-Foam Process Mechanisms.

Hirasaki, G. J., & Lawson, J. B. (1985). Mechanisms of foam flow in porous media: apparent viscosity in smooth capillaries. *Old SPE Journal*, *25*(2), 176-190.

Horozov, T. S. (2008). Foams and foam films stabilised by solid particles. *Current Opinion in Colloid & Interface Science*, *13*(3), 134-140.

Irani, C. A., & Solomon, C. (1986, April). Slim-Tube Investigation of CO2 Foams. In *SPE Enhanced Oil Recovery Symposium*.

Jensen, J. A., & Friedmann, F. (1987, April). Physical and Chemical Effects of an Oil phase on the Propagation of Foam in Porous Media. In *SPE California Regional Meeting*.

Johonnott, E. S. (1906). LXVIII. The black spot in thin liquid films. *The London, Edinburgh, and Dublin Philosophical Magazine and Journal of Science*, *11*(66), 746-753.

Kaptay, G. (2006). On the equation of the maximum capillary pressure induced by solid particles to stabilize emulsions and foams and on the emulsion stability diagrams. *Colloids and Surfaces A: Physicochemical and Engineering Aspects*, *282*, 387-401.

Koval, E. J. (1963). A method for predicting the performance of unstable miscible displacement in heterogeneous media. *Old SPE Journal*, *3*(2), 145-154.

Kovscek, A. R., Patzek, T. W., & Radke, C. J. (1994, April). Mechanistic prediction of foam displacement in multidimensions: A population balance approach. In *SPE/DOE Improved Oil Recovery Symposium*.

Kralchevski, P., Nikolov, A., Wasan, D. T., & Ivanov, I. (1990). Formation and expansion of dark spots in stratifying foam films. *Langmuir*, *6*(6), 1180-1189.

Kuhlman, M. (1990). Visualizing the effect of light oil on CO2 foams. *Journal of Petroleum Technology*, *42*(7), 902-908.

Lake, L. W. (1989). Enhanced oil recovery, Prentice Hall.

Lake, L. W., Schmidt, R. L & Venuto, P. B. (1990). A niche for enhanced oil recovery in the 1990s. *Oil & Gas Journal*, *88*(17), 62-67..

Liu, Q., Zhang, S., Sun, D., & Xu, J. (2010). Foams stabilized by Laponite nanoparticles and alkylammonium bromides with different alkyl chain lengths. *Colloids and Surfaces A: Physicochemical and Engineering Aspects*, *355*(1), 151-157.

Mo, D., Yu, J., Liu, N., & Lee, R. L. (2012, January 1). Study of the Effect of Different Factors on Nanoparticle-Stablized CO2 Foam for Mobility Control. Society of Petroleum Engineers. doi:10.2118/159282-MS

Orr Jr, F. M., Heller, J. P., & Taber, J. J. (1982). Carbon dioxide flooding for enhanced oil recovery: Promise and problems. *Journal of the American Oil Chemists Society*, *59*(10), 810A-817A.

Patzek, T. (1996). Field applications of steam foam for mobility improvement and profile control. *SPE Reservoir Engineering*, *11*(2), 79-86.

Paul, K. T., Satpathy, S. K., Manna, I., Chakraborty, K. K., & Nando, G. B. (2007). Preparation and characterization of nano structured materials from fly ash: A waste from thermal power stations, by high energy ball milling.*Nanoscale Research Letters*, *2*(8), 397-404.

Pugh, R. J. (1996). Foaming, foam films, antifoaming and defoaming. *Advances in Colloid and Interface Science*, *64*, 67-142.

Robinson, J. V., & Woods, W. W. (1948). A method of selecting foam inhibitors. *Journal of the Society of Chemical Industry*, *67*(9), 361-365.

Rossen, W. R. (1996). Foams in enhanced oil recovery. *Surfactant Science Series*, 413-464.

Rossen, W., van Duijn, C., Nguyen, Q., Shen, C., & Vikingstad, A. (2010). Injection strategies to overcome gravity segregation in simultaneous gas and water injection into homogeneous reservoirs. *SPE Journal*, *15*(1), 76-90.

Schramm, L. L., & Novosad, J. J. (1990). Micro-visualization of foam interactions with a crude oil. *Colloids and Surfaces*, *46*(1), 21-43.

Sethumadhavan, G. N., Nikolov, A. D., & Wasan, D. T. (2001). Stability of liquid films containing monodisperse colloidal particles. *Journal of colloid and interface science*, *240*(1), 105-112.

Sethumadhavan, G., Nikolov, A., & Wasan, D. (2004). Stability of films with nanoparticles. *Journal of colloid and interface science*, *272*(1), 167-171.

Taber, J. J., Martin, F. D., & Seright, R. S. (1997). EOR screening criteria revisited-Part 1: Introduction to screening criteria and enhanced recovery field projects. *SPE Reservoir Engineering*, *12*(3), 189-198.

Worthen, A., Bagaria, H., Chen, Y., Bryant, S., Huh, C., & Johnston, K. (2012, April). Nanoparticle Stabilized Carbon Dioxide in Water Foams for Enhanced Oil Recovery. In *SPE Improved Oil Recovery Symposium*.

Worthen, A. J., Bryant, S. L., Huh, C., & Johnston, K. P. (2013). Carbon dioxide-in-water foams stabilized with nanoparticles and surfactant acting in synergy. *AIChE Journal*.

Yu, J., An, C., Mo, D., Liu, N., & Lee, R. (2012, April). Foam Mobility Control for Nanoparticle-Stabilized Supercritical CO2 Foam. In *SPE Improved Oil Recovery Symposium*.

Zhang, R., & Somasundaran, P. (2006). Advances in adsorption of surfactants and their mixtures at solid/solution interfaces. *Advances in colloid and interface science*, *123*, 213-229.

Zhang, S., Sun, D., Dong, X., Li, C., & Xu, J. (2008). Aqueous foams stabilized with particles and nonionic surfactants. *Colloids and Surfaces A: Physicochemical and Engineering Aspects*, *324*(1), 1-8.